The Astrophysical Journal, 812:3 (12pp), 2015 October 10 doi:10.1088/0004-637X/812/1/3

AN ACTIVITY–ROTATION RELATIONSHIP AND KINEMATIC ANALYSIS OF NEARBY MID-TO-LATE-TYPE M DWARFS

Andrew A. West[1], Kolby L. Weisenburger[1,2], Jonathan Irwin[3], Zachory K. Berta-Thompson[4], David Charbonneau[3], Jason Dittmann[3], and J. Sebastian Pineda[5]

[1] Department of Astronomy, Boston University, 725 Commonwealth Ave, Boston, MA 02215, USA; aawest@bu.edu
[2] Department of Astronomy, University of Washington, Box 351580, Seattle, WA 98195, USA
[3] Harvard-Smithsonian Center for Astrophysics, 60 Garden St., Cambridge, MA 02138, USA
[4] MIT, Kavli Institute for Astrophysics and Space Research, 77 Massachusetts Ave., Bldg. 37, Cambridge, MA 02139, USA
[5] California Institute of Technology, Department of Astronomy, 1200 E. California Ave, Pasadena, CA 91125, USA

Received 2015 February 12; accepted 2015 August 22; published 2015 October 2

ABSTRACT

Using spectroscopic observations and photometric light curves of 238 nearby M dwarfs from the MEarth exoplanet transit survey, we examine the relationships between magnetic activity (quantified by Hα emission), rotation period, and stellar age. Previous attempts to investigate the relationship between magnetic activity and rotation in these stars were hampered by the limited number of M dwarfs with measured rotation periods (and the fact that v sin i measurements probe only rapid rotation). However, the photometric data from MEarth allows us to probe a wide range of rotation periods for hundreds of M dwarf stars (from shorter than one to longer than 100 days). Over all M spectral types that we probe, we find that the presence of magnetic activity is tied to rotation, including for late-type, fully convective M dwarfs. We also find evidence that the fraction of late-type M dwarfs that are active may be higher at longer rotation periods compared to their early-type counterparts, with several active, late-type, slowly rotating stars present in our sample. Additionally, we find that all M dwarfs with rotation periods shorter than 26 days (early-type; M1–M4) and 86 days (late-type; M5–M8) are magnetically active. This potential mismatch suggests that the physical mechanisms that connect stellar rotation to chromospheric heating may be different in fully convective stars. A kinematic analysis suggests that the magnetically active, rapidly rotating stars are consistent with a kinematically young population, while slow-rotators are less active or inactive and appear to belong to an older, dynamically heated stellar population.

Key words: stars: activity – stars: chromospheres – stars: kinematics and dynamics – stars: late-type – stars: low-mass – stars: rotation

Supporting material: machine-readable table

1. INTRODUCTION

Many late-type M dwarfs (>M4) have strong magnetic fields that can exceed 1 kG and heat their stellar chromospheres and coronae, creating "magnetic activity" that is observed from the radio to the X-ray (e.g., Hawley et al. 1996; West et al. 2004; Berger et al. 2008; Reiners & Basri 2008, 2009; Williams et al. 2014). Although magnetic activity has been observed in M dwarfs for decades, the exact mechanism that gives rise to the chromospheric and coronal heating is still not well-understood. The production of magnetic fields and the subsequent activity may play a vital role in the habitability of attending planets, which may be numerous given the ubiquity of M dwarfs as planet hosts in the Galaxy (e.g., Charbonneau et al. 2009; Muirhead et al. 2012; Dressing & Charbonneau 2013, 2015). In addition, given their fully convective interiors, late-type M dwarfs serve as important laboratories for studying magnetic dynamo generation in stellar (and potentially planetary) environments and are vital for understanding the role that various stellar properties play in the magnetic field and activity generation in low-mass stars.

In solar-type stars, magnetic field generation and subsequent heating are closely tied to stellar rotation; the faster a star rotates, the stronger its magnetic heating and surface activity. Angular momentum loss from magnetized winds slows rotation in solar-type stars, and as a result, magnetic activity decreases with age. These effects have been studied for decades, producing ample evidence for a strong connection between age, stellar rotation, and magnetic activity in solar-type stars (e.g., Skumanich 1972; Barry 1988; Soderblom et al. 1991; Barnes 2003; Pizzolato et al. 2003; Mamajek & Hillenbrand 2008). All indications suggest that this connection between age, rotation, and activity extends to early-type M dwarfs (<M4), where rotation and activity are strongly correlated (e.g., Mohanty & Basri 2003; Pizzolato et al. 2003; Kiraga & Stepien 2007). The finite active lifetimes of early-type M dwarfs observed in nearby clusters suggest that age continues to play an important role in the rotation and magnetic activity evolution of low-mass stars (Stauffer et al. 1994; Hawley et al. 1999).

At a spectral type of about M4, stars become fully convective (0.35 $M_{\odot}$; Chabrier & Baraffe 1997; Reid & Hawley 2005), a property that may affect how magnetic field (and the resulting heating) is generated. Despite this change, magnetic activity persists in late-type M dwarfs; the fraction of active M dwarfs peaks around a spectral type of M7 before decreasing into the brown dwarf regime (Hawley et al. 1996; Gizis et al. 2000; West et al. 2004). Several studies have demonstrated that the large fraction of late-type M dwarfs observed to be active is likely a result of their long activity lifetimes (Silvestri et al. 2005; West et al. 2008).

Using 37,845 M dwarfs from the Sloan Digital Sky Survey (York et al. 2000), West et al. (2006, 2008) found that stars farther from the Galactic plane were less likely to be magnetically active (as traced by Hα) than those near the plane. They interpreted the change in the activity fraction as an

effect of age: as stars pass through the Galactic plane, they are dynamically heated by gravitational interactions and obtain orbits that take them farther from the plane. Therefore, stars close to the Galactic plane are statistically younger, while stars farther away are statistically older. West et al. (2008) quantified this "Galactic stratigraphy" using a one-dimensional (1D) dynamical model and derived the Hα activity lifetimes for M0–M7 dwarfs, finding that early-type M dwarfs (with both radiative and convection zones) have active lifetimes of 1–2 Gyr, while late-type M dwarfs (with fully convective interiors) have active lifetimes that exceed 7 Gyr. The level of activity (as quantified by the ratio of the luminosity in Hα to the bolometric luminosity—$L_{\rm H\alpha}/L_{\rm bol}$) also appears to decrease as a function of stratigraphic age for all M dwarfs (early and late-type), confirming that an age–activity relation persists into the fully convective regime (West et al. 2008).

Tying activity (and age) to rotation for late-type M dwarfs has been more challenging. Recent simulations of dynamos find that rotation may play a significant role in the magnetic field generation of fully convective stars (Dobler et al. 2006; Browning 2008). From a simple analytical model, Reiners & Mohanty (2012) suggest that the age–rotation relation extends to late-type M dwarfs and that the angular momentum evolution of all stars is more a function of stellar radius than it is interior structure. Indeed, a few empirical studies have uncovered evidence that activity and rotation might be linked in late-type M dwarfs (Delfosse et al. 1998; Mohanty & Basri 2003; Reiners & Basri 2008; Browning et al. 2010; Reiners & Mohanty 2012). However, the majority of the observations have relied on high-resolution spectroscopic data, which measure the rotational velocity modified by the inclination of the star (v sin i). While v sin i measurements provide important clues to the underlying stellar rotation, they have a couple of limitations: (1) the best spectrographs can produce v sin i values only down to about 1 km s^{-1}, which for a 0.2 $R_\odot$ star corresponds to a rotation period of 10 days, and are therefore completely insensitive to slowly rotating stars; and (2) the inclination dependence adds significant scatter to the derived rotation velocities. Previous results demonstrate these limitations by showing that almost all late-type M dwarfs with a detected v sin i have the same "saturated" level of magnetic activity; slowly rotating M dwarfs with potentially less magnetic activity are not detectable.

An alternative method for studying stellar rotation is to use photometrically derived rotation periods (e.g., Kiraga & Stepien 2007). Periodic signals result from brightness variations caused by long-lived spots on the stellar surface rotating in and out of view. While v sin i observations require a single spectroscopic observation, observing periodic, photometric variability requires numerous, high-cadence observations that have been historically prohibitive for large samples of late-type M dwarfs. However, recent programs to search for transiting planets around late-type M dwarfs have produced large catalogs of time-domain photometry from which can be gleaned several important stellar properties, including rotation periods (Irwin et al. 2009a; Law et al. 2012).

One of these transit programs, the MEarth Project[6] (Nutzman & Charbonneau 2008; Irwin et al. 2009b, 2011b; Berta et al. 2012), is employing two arrays of robotic telescopes to photometrically monitor 4000 nearby, mid-to-late M dwarfs. MEarth data and associated observations have provided new measurements of the fundamental properties of nearby mid-to-late M dwarfs, including their distances (Dittmann et al. 2014) and their near-infrared spectra (Newton et al. 2014). Early in the survey, Irwin et al. (2011a) determined photometric rotation periods (ranging from 0.28 to 154 days) for 41 of the MEarth M dwarfs with known parallaxes, and identified a relationship between these rotation periods and kinematic age. As the mid-to-late M dwarfs observed by MEarth are nearby and therefore relatively bright, it is possible to obtain a larger sample of optical spectroscopy to probe magnetic activity, thus enabling a robust investigation of how the rotation–activity relation for fully convective M dwarfs extends to slowly rotating stars.

Determining ages for stars can be particularly challenging, especially for low-mass stars (Soderblom 2010). In the past, age-dependent relations for stars have been calibrated using stellar clusters. However, the faintness of M dwarfs and the large distances to stellar clusters with ages $>$1 Gyr preclude any detailed observations of low-mass stars in the cluster environment. One alternative method for probing stellar age is to use the three-dimensional (3D) stellar kinematics of a population. Historically, the dynamics of stars have been used to estimate ages, as dynamical interactions cause the orbits of older stars to become more elliptical and inclined to the Galactic plane (Wilson & Woolley 1970; Eggen & Iben 1989; Leggett 1992). Specifically, stars that exhibit larger velocity dispersions have likely experienced more dynamical encounters with molecular clouds and/or other stars and are therefore older. This is particularly true in the vertical or W direction of stellar motion since most stars begin their lives in the Galactic disk and slowly diffuse away via dynamical heating (West et al. 2006). Older stars also have slower azimuthal or V mean velocities due to asymmetric drift (e.g., Eggen & Iben 1989). While using stellar kinematics to determine ages of individual stars is highly problematic (since the dynamical processes that affect individual stellar orbits are stochastic), 3D motions can reveal important age information for bulk populations. Dynamical analyses do require large samples, which until recently have not been available for late-type M dwarfs.

In this paper, we use an expanded sample of MEarth rotation periods for nearby M dwarfs, new optical spectroscopy of these targets, and their full space motions to investigate the rotation–activity and rotation–activity–age relation for late-type M dwarfs. Section 2 describes the determination of rotation periods from MEarth data and the determination of magnetic activity from optical spectroscopic observations. We describe the rotation, activity, and kinematic analysis in Section 3. In Section 4 we demonstrate that there is a close tie between rotation and activity and that the slowest rotators come from a dynamically older population. Lastly, Section 5 summarizes our conclusions and gives a brief discussion.

2. DATA

2.1. Rotation Periods from MEarth Photometry

To measure M dwarf rotation periods, we use photometric observations from the MEarth survey for transiting exoplanets (see Nutzman & Charbonneau 2008; Berta et al. 2012). MEarth comprises two telescope arrays, each consisting of eight robotic telescopes. All of the data in this paper come from the MEarth-north array at the Fred Lawrence Whipple Observatory (FLWO) at Mt. Hopkins, AZ, which has been gathering data

[6] http://cfa.harvard.edu/MEarth/

since 2008. The MEarth team recently commissioned a duplicate array at Cerro Tololo Interamerican Observatory (CTIO), called MEarth-south. Because the new array started regular observations only in 2014 January, data from MEarth-south are not included in the following analyses. The MEarth M dwarf light curves used in this paper (along with the full MEarth sample) are publicly available for download from the MEarth website.[7]

The sample of M dwarfs observed by MEarth was designed to maximize sensitivity to the detection of small transiting planets (2–4 $R_{\oplus}$), as detailed in Nutzman & Charbonneau (2008). The MEarth sample is heavily biased toward mid-to-late M dwarfs within 33 pc, with most stars having spectral types of M4–M6 but also including several stars of earlier and later spectral types. This paper makes use of the MEarth sample of stars and inherits the selection criteria of the planet-search survey. While the sample of stars observed was not designed explicitly to probe rotation across the entire M dwarf spectral class, it spans a sufficient range of spectral types to enable interesting comparisons between earlier (which in this paper refers primarily to M3–M4) and later (primarily M5–M6) spectral types.

The MEarth telescopes are 40 cm in diameter and equipped with back-illuminated CCDs. The telescopes observe automatically whenever conditions allow, with an adaptive scheduling algorithm selecting targets from a prioritized queue. The rotation periods in this paper are derived from "planet cadence" observations, in which a star is observed once every 10–30 minutes for at least one observational season, resulting in light curves containing hundreds to a few thousand data points. For some stars, up to three observational seasons contributed to the rotation analysis. We took care to minimize changes to the telescopes to preserve long term stability, but those changes that were necessary are summarized in Berta et al. (2012) and documented in detail in the notes associated with the MEarth data releases.

The MEarth-north bandpass is fixed and nearly identical across the eight telescopes. Designed to maximize photon flux from red M dwarf targets, the bandpass is wide and has a shape set at short wavelengths by a longpass filter that cuts on at 715 nm and at long wavelengths by the quantum efficiency of the CCD, which decreases significantly by about 1000 nm. The time-variable optical depth through strong telluric water vapor features that fall within the MEarth bandpass can cause systematic photometric trends in MEarth M dwarf light curves, but the effect can be mitigated through an empirical correction (Berta et al. 2012). Photometric modulations due to rotating starspots are relatively muted in the MEarth bandpass compared to bluer wavelengths, but they can still have readily detectable peak-to-peak amplitudes of up to several percent (Irwin et al. 2011a).

Rotation periods were extracted using a weighted least-squares periodogram fitting algorithm that corrects for and marginalizes over systematic photometric trends, including those caused by varying telluric water absorption. This analysis is described in detail in Irwin et al. (2011a). Whereas Irwin et al. (2011a) included rotation periods only for stars with published literature parallaxes, here we extend the sample to all M dwarfs with rotational modulations detectable in the MEarth photometry that were available up to 2011, resulting in 164 targets. For this paper's analysis, we applied a two-tier classification system ("1" and "2") for all of the measured rotation periods, with "1" being the most robust detections. Some of the reasons that rotation periods were given a classification of "2" were if the stars had long periods and less than two complete cycles were observed or if the stars had larger uncertainties in the phase folding procedure. We were unable to measure rotation periods for all of the MEarth stars. For stars with detected rotation periods, the amplitude of the photometric modulations were typically 0.5%–2% peak-to-peak. Irwin et al. (2011a) made initial attempts to characterize the reliability and contamination of rotation period detection with MEarth and found the selection to be fairly clean for stars with >1% variability, but messy (and strongly period-dependent) for stars showing variability of 0.5% or less. Figure 1 shows the distribution of measured rotation periods for all of the M dwarfs with spectroscopic observations. The periods used in this paper can be found in Table 1. A complete catalog of rotation periods from the MEarth survey will be included in a future publication (E.R. Newton et al. 2015, in preparation).

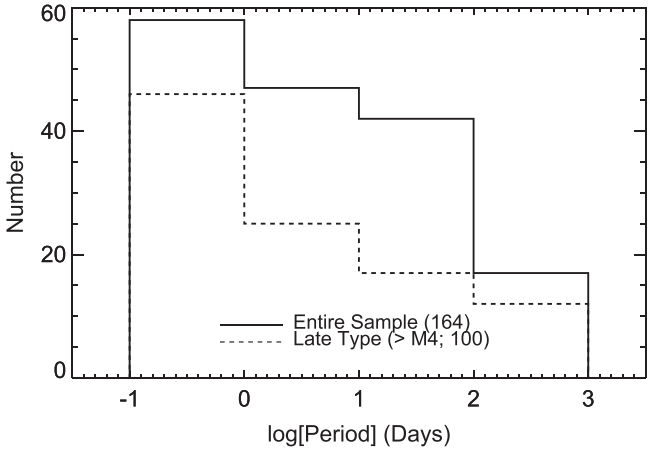

Figure 1. Distribution of rotation periods for all MEarth M dwarfs (solid) and late-type (>M4) M dwarfs (dashed) with spectroscopic observations.

2.2. Magnetic Activity from FAST Spectroscopy

To probe the magnetic activity of this sample, we obtained optical spectra for 238 MEarth M dwarfs. The sample of stars observed spectroscopically included those with measured rotation periods, as well as additional M dwarfs for which no rotational modulations were detected. Observed using the 600 lines mm^{-1} grating on the FAST spectrograph on the 1.5 m Tillinghast Telescope at FLWO, the spectra have a resolution of $R = 3000$. The spectra cover 5550–7550 Å and include several features that are important for M dwarf analyses, including (but not limited to) the CaH and TiO molecular bands and the Hα atomic line.

The FAST observations were acquired over 30 nights from 2010 December to 2012 July, with HeNeAr lamp exposures taken at every telescope position and spectrophotometric standards observed every night. Exposures lasted typically about five minutes, yielding signal-to-noise ratios (S/N) of about 50 per resolution element. With a scripted IRAF reduction, we bias-subtracted and flat-fielded all spectra using calibration exposures taken every time the instrument grating changed, and applied a wavelength calibration determined for

[7] http://cfa.harvard.edu/MEarth/Data.html

Table 1
Kinematics, Activity, and Rotation Periods for MEarth M Dwarfs[a]

Name	R.A.	Decl.	Spectral Type	Distance[a] (pc)	Distance[a] Flag	Radial Vel. (km s^{-1})	$PM_{R.A.}$[b] (mas yr^{-1})	$PM_{Decl.}$[b] (mas yr^{-1})	U[c] (km s^{-1})	V[c] (km s^{-1})	W[c] (km s^{-1})	Period (days)	Hα EW[d] (Å)	Activity Flag[e]	Rotation Flag[f]
LSPMJ0001+0659	00:01:15.809	+06:59:35.65	M6	16.7	D	−0.7	−447	−81	+11.1 ± 1.5	+0.1 ± 8.4	+13.8 ± 4.6	20.4	+6.9 ± 1.2	1	1
LSPMJ0015+4344	00:15:18.827	+43:44:34.72	M5	25.7	L	+5.9	+232	+38	+10.1 ± 4.1	+4.6 ± 8.3	+7.1 ± 2.8	1.4	+6.5 ± 0.8	1	1
LSPMJ0015+1333	00:15:49.244	+13:33:22.25	M3	9.6	D	+65.1	+621	+333	+0.2 ± 2.2	+32.1 ± 8.3	−25.4 ± 4.3	⋯	⋯	0	0
LSPMJ0016+1951E	00:16:16.141	+19:51:50.56	M4	22.2	L	+9.0	+709	−748	+10.3 ± 2.8	+4.1 ± 8.3	+7.9 ± 4.1	⋯	⋯	0	0
LSPMJ0016+2003	00:16:56.803	+20:03:55.17	M4	22.2	L	+12.0	+228	+24	+9.2 ± 2.8	+6.9 ± 8.3	+5.2 ± 4.0	17.3	+3.5 ± 0.4	1	1
LSPMJ0018+2748	00:18:53.590	+27:48:49.81	M4	19.2	L	+12.7	+387	−101	+8.5 ± 3.3	+8.3 ± 8.3	+4.5 ± 3.6	6.0	+1.6 ± 0.3	1	1
LSPMJ0024+2626	00:24:03.799	+26:26:29.76	M4	26.1	D	+16.0	+162	−55	+8.3 ± 3.5	+8.5 ± 8.3	+4.2 ± 3.7	29.9	+1.3 ± 0.4	1	1
LSPMJ0024+3002	00:24:34.876	+30:02:29.59	M5	15.5	D	+17.6	+580	+28	+7.1 ± 3.6	+10.8 ± 8.3	+2.9 ± 3.4	1.1	+6.6 ± 0.9	1	1
LSPMJ0028+5022	00:28:53.972	+50:22:33.17	M4	16.9	D	+24.2	+423	+124	+2.8 ± 4.6	+17.8 ± 8.3	+3.8 ± 1.8	1.1	+5.9 ± 0.6	1	1
LSPMJ0033+1448	00:33:22.350	+14:48:06.45	M5	27.3	D	+21.5	+278	−71	+6.7 ± 3.1	+11.6 ± 8.2	−1.2 ± 4.2	0.4	+3.5 ± 0.6	1	2
LSPMJ0035 +5241N	00:35:53.680	+52:41:36.59	M4	⋯	L	+12.7	+787	−186	⋯	⋯	⋯	⋯	⋯	0	0
LSPMJ0038+6150	00:38:27.677	+61:50:06.34	M4	46.5	D	−58.3	+349	−43	+37.5 ± 5.1	−40.1 ± 8.2	+7.9 ± 1.2	62.4	⋯	0	2
LSPMJ0039+1454S	00:39:33.544	+14:54:18.96	M4	⋯	L	+9.1	+321	+39	⋯	⋯	⋯	34.0	⋯	0	1
LSPMJ0103+6221	01:03:19.824	+62:21:55.74	M6	10.5	L	+6.7	+739	+86	+9.3 ± 5.4	+5.9 ± 7.9	+7.0 ± 0.5	1.0	+9.2 ± 1.3	1	1
LSPMJ0130+0236	01:30:43.122	+02:36:37.01	M6	18.3	D	−15.6	−119	−194	+18.3 ± 4.1	−1.5 ± 7.6	+24.3 ± 4.6	⋯	+0.8 ± 0.5	1	0
LSPMJ0153+0147	01:53:30.754	+01:47:55.89	M6	20.1	D	+30.4	+427	+45	+1.4 ± 4.7	+9.4 ± 7.2	−8.2 ± 4.6	0.2	+8.6 ± 1.2	1	1
LSPMJ0153+4427	01:53:49.551	+44:27:28.49	M5	20.1	D	+14.3	+245	−92	+6.4 ± 6.5	+8.6 ± 7.1	+5.4 ± 0.7	0.2	+17.8 ± 2.3	1	1
LSPMJ0158+4049	01:58:45.211	+40:49:44.51	M5	17.1	D	+19.1	+399	−69	+3.5 ± 6.5	+11.1 ± 7.0	+3.7 ± 0.9	0.5	+7.3 ± 1.0	1	1
LSPMJ0202+1334	02:02:44.355	+13:34:33.21	M5	20.7	D	+15.6	+461	−111	+6.7 ± 5.7	+7.0 ± 7.0	+3.0 ± 3.5	4.0	+7.6 ± 0.9	1	1
LSPMJ0212+0000	02:12:54.624	+00:00:16.71	M4	9.8	D	+33.0	+560	+34	+0.5 ± 5.1	+8.0 ± 6.7	−8.1 ± 4.7	4.7	+2.2 ± 0.4	1	1
⋯	⋯	⋯	⋯	⋯	⋯	⋯	⋯	⋯	⋯	⋯	⋯	⋯	⋯	⋯	⋯

Notes. The machine-readable table also contains the semiamplitudes of the rotation data as well as other extracted parameters from the spectra used in this paper, including a calculation of $L_{H\alpha}/L_{bol}$ and atomic/molecular indices for Na, TiO, CaH, and CaOH features (as defined in Reid et al. 1995).

[a] A Distance Flag of "D" indicates the distance is a trigonometric parallax measurement derived from MEarth imaging, as published in Dittmann et al. (2014). A flag of "L" indicates the distance comes from Lépine et al. (2005) and may be either photometric, spectroscopic, or trigonometric.

[b] Proper motions are quoted as projected on the plane of the sky, with $(PM_{R.A.}, PM_{Decl.}) = (\mu_\alpha \cos\delta, \mu_\delta)$.

[c] *UVW* velocities are quoted in a right-handed coordinate system, with *U* pointed toward the Galactic center.

[d] This table uses a convention in which emission lines correspond to equivalent widths >0.

[e] Active M dwarfs have an Active Flag value of 1; inactive stars have a flag of 0 (see Section 3.1).

[f] Stars with measured rotation periods have a Rotation Flag value of 1 or 2, with a value of 1 being more robust. Stars whose rotation periods did not cross our detection threshold are flagged as 0 (see Section 2.1).

(This table is available in its entirety in machine-readable form.)

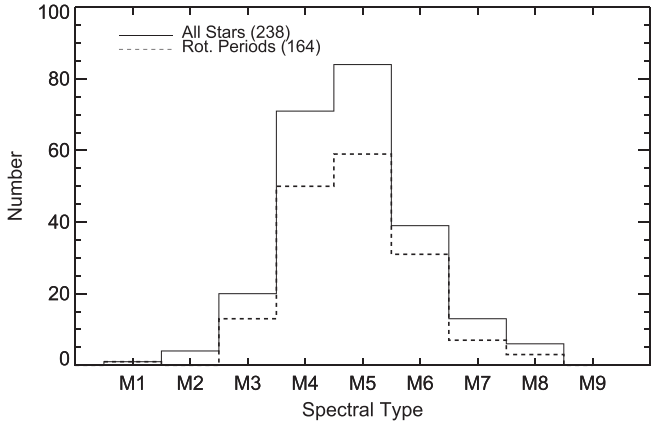

Figure 2. Distribution of spectral types for MEarth stars with FAST spectroscopic observations, including stars with measured rotation periods (dashed).

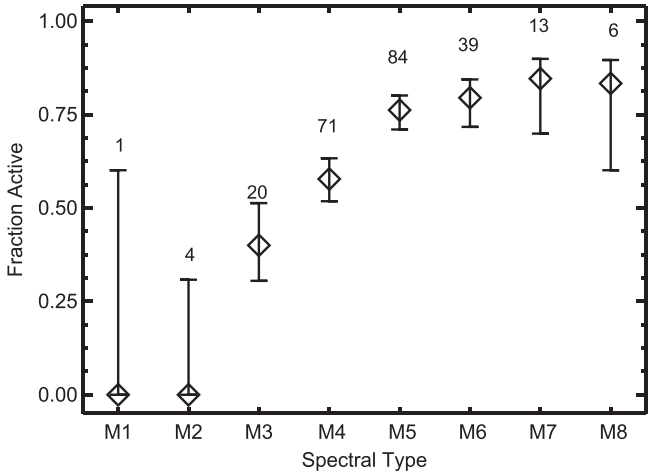

Figure 3. Fraction of magnetically active M dwarfs as a function of spectral type. Errors were computed from binomial statistics and the numbers above each symbol indicate the total number of stars (active + inactive) in each bin. Similar to previous results, we see a dramatic increase in the fraction of active M dwarfs with increasing spectral type.

each spectrum from its matching HeNeAr exposure. We extracted 1D spectra for each target, weighting by the profile in the cross-dispersion direction and using linear interpolation to subtract the sky. We determined a rough flux calibration for each spectrum using the nightly spectrophotometric standards.

2.3. Distances from MEarth Astrometry and Other Sources

To characterize the basic properties of the target M dwarfs, we used distance measurements from several sources. Dittmann et al. (2014) used MEarth imaging to measure geometric parallaxes for 1507 M dwarfs in the MEarth sample. These include 150 out of the 164 stars in the rotation sample and 213 out of the 238 M dwarfs in the spectroscopic sample. For the remaining stars without MEarth parallaxes, we adopted distances published in Lépine et al. (2005), which come either from literature trigonometric parallaxes or from photometric parallax estimates. Proper motions for all of the stars were measured as part of the LSPM-north catalog (Lépine & Shara 2005).

3. ANALYSIS

The FAST spectra were processed with the Hammer spectral-typing facility (Covey et al. 2007). The Hammer uses measurements of atomic and molecular features to estimate an initial spectral type. We then visually inspected all of the spectra with the Hammer (v. 1_2_5) "eye check" function, and manually assigned spectral types to each star—we identified and classified 238 M dwarfs (see Figure 2). Of the 238 M dwarfs for which we obtained FAST spectroscopy, 164 have measured rotation periods.

We measured radial velocities (RVs) by cross-correlating each FAST M dwarf spectrum (between 5600–7100 Å) with the respective Bochanski et al. (2007b) M dwarf template (Mohanty & Basri 2003; West & Basri 2009). We determined the typical uncertainty in our RV by comparing our calculated RVs for 11 stars with previously determined RVs from high-resolution spectra (Delfosse et al. 1998; Montes et al. 2001; Nidever et al. 2002; Mohanty & Basri 2003; Browning et al. 2010; Shkolnik et al. 2010). The RMS difference between the RV measurements was 5.1 km s^{-1}, which we took as the uncertainty in our ability to measure RVs from the FAST spectra. Each spectrum was corrected to air wavelengths in a zero-velocity heliocentric rest frame for the measurements of spectral features (see below).

3.1. Magnetic Activity

Using the RV-corrected spectra, we determined the presence and magnitude of magnetic activity by measuring Hα equivalent widths (EWs) as defined by West et al. (2011). We used 6500-6550 and 6575–6625 Å as our two continua regions, with the central Hα wavelength at 6562.8 Å. In previous studies, stars with Hα EWs greater than 0.75 Å were considered magnetically active (West et al. 2011). However, given the relatively small size of our FAST sample, we were able to visually inspect each spectrum and classified all stars with detectable Hα emission as "magnetically active." All of the active stars in our sample have Hα EWs $>$ than the 0.75 Å criterion from West et al. (2011), and would have been selected as "active" using an automatic EW threshold. The high S/N of the FAST spectra allowed us to be sensitive to Hα EWs far below the values measured for the active stars in our analysis (particularly for the M3–M6 dwarfs), indicating that we could have detected activity in many of the "inactive" stars had it been present.

M dwarfs that exhibit weak magnetic activity can show Hα in absorption rather than emission (Stauffer & Hartmann 1986; Walkowicz & Hawley 2009). As such, using Hα emission as an activity indicator will not include M dwarfs with the weakest levels of magnetic activity. Throughout this paper, we define active stars as those that exhibit Hα in emission and are therefore strongly magnetically active. We examined all of the inactive early-type M dwarf spectra to look for Hα absorption, and found no evidence for strong absorption. In 9 of 47 of these cases, there were hints of weak Hα absorption. However, a strong nearby TiO absorption feature precluded firm detections, given the low resolution of the FAST spectra. Activity fractions reported in this paper may be slightly higher in reality, because we may have excluded weakly active M dwarfs that do not show Hα in emission.

We identified 160 active M dwarfs, which comprises 67% of the M dwarfs in the spectroscopic sample. Figure 3 shows the fraction of magnetically active M dwarfs in our sample as a

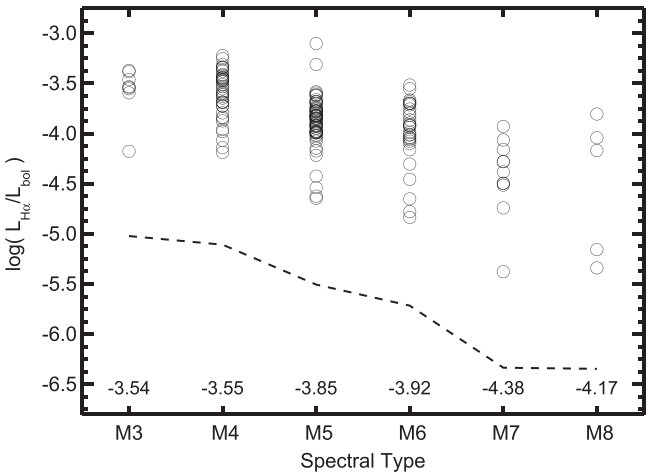

Figure 4. $L_{H\alpha}/L_{bol}$ as a function of spectral type for active stars in the sample. Spectral types earlier than M3 are not shown, as our sample contains no such stars that are active. Median values of $\log(L_{H\alpha}/L_{bol})$ are listed below. The dashed line indicates the typical $L_{H\alpha}/L_{bol}$ values to which we are sensitive as a function of spectral type. There is a large spread in the $L_{H\alpha}/L_{bol}$ values at each spectral type, as well as a significant decrease in the median $L_{H\alpha}/L_{bol}$ values with increasing spectral type.

function of spectral type. As seen in previous studies (Hawley et al. 1996; Gizis et al. 2000; West et al. 2004), we see an increase in activity with increasing spectral type, which is likely due to the longer active lifetimes of late-type M dwarfs (West et al. 2008).

There were previously determined Hα EW values for 23 of the stars in our sample (Reid et al. 1995). We compared the FAST EWs to those from Reid et al. (1995) and found that 12 of the measurements are within 13% of those previously reported, with the median difference being 14% for all stars. Six of the stars have EWs that are different by more than 25% and only two show variations larger than 50%. Variation on this level can be explained by the typical variation of Hα emission in M dwarfs (e.g., Bell et al. 2012). With the activity criterion used in this paper, none of the 23 stars switch from being active to being inactive (or vice versa) between the two epochs.

For the active stars in the sample (those with Hα emission), we calculated the magnetic activity strength, $L_{H\alpha}/L_{bol}$ using the χ factor from Walkowicz et al. (2004). We multiplied the spectral type-dependent conversion factor χ by the Hα EW to get the ratio $L_{H\alpha}/L_{bol}$. Figure 4 shows the $L_{H\alpha}/L_{bol}$ values as a function of spectral type. The dashed line in Figure 4 indicated the typical level of Hα emission to which we are sensitive as a function of spectral type. This detection threshold was estimated using the typical noise level near Hα in the FAST spectra and assuming a detectable emission line would have a peak that is at least three times larger than the noise. As shown in previous studies (e.g., Burgasser et al. 2002; West et al. 2004), we see a decrease in $L_{H\alpha}/L_{bol}$ with increasing spectral type (well above detection threshold for M3–M6 dwarfs; dashed line) as well as a large spread of $L_{H\alpha}/L_{bol}$ at each spectral type. The latter is a combination of the intrinsic spread of the active M dwarf population and age-dependent effects on the activity that are washed out when stars of different ages are binned together.

As part of our analysis, we also measured the TiO, CaH, and CaOH molecular bandheads as defined by Reid et al. (1995), and the Na I atomic absorption line. All of the values can be found in the online version of Table 1.

3.2. Kinematics

We combined the stellar positions, proper motions, distances, and RVs to compute the Galactic U, V, W velocities for 212 of the stars in our sample.[8] We corrected for the solar motion with respect to the Local Standard of Rest (11, 12, 7 km s^{-1}; Schönrich et al. 2010) and propagated our measurement errors through to formal uncertainties in U, V, and W using a modified version of the IDL routine `GAL_UVW.PRO`.

There were 159 stars in our sample that had both good rotation measurements (flags "1" or "2" from Section 2) and 3D space motions. We divided these stars into four different bins based on the rotation velocities (<1 days, 1–10 days, 10–100 days, and >100 days; with 58, 47, 42, and 17 stars in each bin, respectively).

The velocity distributions of specific stellar populations can be modeled by Gaussian distributions in all three kinematic components. Mean space velocities and their respective spreads and uncertainties are often calculated using fits to cumulative probability distributions or simple Gaussian fits to velocity histograms (Reid et al. 1995; Bochanski et al. 2007a; Reiners & Basri 2009). However, these methods are computationally intensive and/or heavily biased by the binning strategy. The challenges associated with previous methods are amplified when the data are sparse, which is particularly important for our small number of slow rotators.

Alternatively, under the assumption that the underlying velocity distribution is Gaussian, probabilities for a given model mean and standard deviation can be computed analytically and compared to the data using a Bayesian approach. For a given subset of velocities, the joint probability distribution for the best-fit mean (μ) and standard deviation (σ) of the population is given by:

$$p(\{\mu, \sigma\}; \{\text{data}\}) \propto p(\{\text{data}\}; \{\mu, \sigma\}) p(\{\mu, \sigma\}), \quad (1)$$

where the first term on the right represents the likelihood of the data and the second term on the right is the prior distribution of parameters, which we took to be uninformative.[9]

The likelihood is the product of the probabilities for all of the data points in a subset, where the probability for each datum is given by the Gaussian distribution:

$$p\left(\{m, s\}_i; \{\mu, \sigma\}\right) = \frac{1}{\sqrt{2\pi\left(\sigma^2 + s_i^2\right)}} \exp\left[\frac{-(m_i - \mu)^2}{2\left(\sigma^2 + s_i^2\right)}\right], \quad (2)$$

where m and s are the measured velocity and uncertainty of a single star, p is the probability that the datum comes from a Gaussian distribution described by μ and σ, and the index i runs over all stars within a bin if it contains at least three stars.

We constructed a grid of μ and σ values and explored the joint probability distribution of Equation (1) for the four kinematic sub-samples at each of the grid points. From the resulting peaks of the joint probability density distributions, we computed μ and σ values for each rotation/activity sub-sample. We also calculated realistic uncertainties from the spread of the marginalized distributions for each parameter. The results of

[8] We used a right-handed coordinate system with U pointed toward the Galactic center.

[9] We used the Jeffreys prior, $1/\sigma$, also known as the logarithmic prior, for the standard deviation and a flat prior for the mean.

Table 2
Population Kinematics—Entire Sample

Mean Rotation Period (days)	μ_U (km s^{-1})	μ_V (km s^{-1})	μ_W (km s^{-1})	σ_U (km s^{-1})	σ_V (km s^{-1})	σ_W (km s^{-1})
0.5	$9.8^{0.3}_{1.3}$	$3.9^{0.7}_{0.8}$	$5.0^{1.0}_{0.9}$	...	$4.5^{0.6}_{0.5}$	$7.2^{0.8}_{0.7}$
3.3	$5.6^{1.3}_{1.3}$	$3.9^{1.3}_{1.3}$	$9.2^{1.4}_{1.4}$	$8.8^{1.6}_{1.5}$	$8.4^{1.0}_{0.9}$	$9.8^{1.1}_{0.9}$
49.0	$2.2^{2.2}_{2.1}$	$-0.3^{1.7}_{1.6}$	$14.4^{2.0}_{1.9}$	$14.2^{1.9}_{1.7}$	$10.2^{1.4}_{1.2}$	$13.2^{1.5}_{1.2}$
119.8	$8.9^{1.8}_{2.0}$	$-1.4^{2.6}_{2.4}$	$8.1^{3.7}_{3.8}$	$6.3^{2.1}_{1.7}$	$7.4^{2.2}_{1.7}$	$14.6^{3.4}_{2.4}$

this analysis can be found in Table 2 and are discussed below in more detail. For the fastest rotators, the data did not provide a good constraint on the U velocity dispersion; that value was excluded from Table 2.

4. RESULTS

4.1. Rotation versus Activity

From the sample of 164 M dwarfs with measured rotation periods, 127 were classified as magnetically active. We investigated how the activity fraction varies as a function of rotation period by dividing the sample into four logarithmically spaced rotation bins (<1 days, 1–10 days, 10–100 days, and >100 days). We also used the Adaptive Kernel Density Estimation routine `akj` within the `quantreg` package in R to construct probability density functions (PDF) for the active and inactive stars as a function of rotation period (R Core Team 2014; Koenker 2015). We then combined the active and inactive PDFs to compute a PDF for the activity fraction as a function of rotation period. We determined confidence intervals (68% and 95%) by taking 5000 bootstrap samples of the data. Figure 5 shows the activity fraction as a function of rotation period for the logarithmic bins (diamonds) and the nonparametric PDF (gray shading). Figure 5 indicates that all M dwarfs with periods shorter than 10 days show detectable Hα emission, with a decrease in activity fraction as a function of increasing rotation period. While the slowest rotating M dwarfs have lower activity fractions, there appears to be a small population of active, slowly rotating stars.

We further explored the rotation dependence on activity fraction by dividing the sample into early (M1–M4) and late-type (M5–M8) samples. Figure 6 was made using the same procedures as in Figure 5 except that we used 2000 bootstrap samples to determine the PDF confidence intervals. Figure 6 demonstrates a clear difference in the populations with the early-type M dwarfs (left) showing a strong decrease in activity fraction with increasing rotation period, with the slowest rotators being completely inactive. The activity fraction of the late-type population (right) stays very high for stars with rotation periods shorter than 100 days, after which it decreases. A small number of the slowest rotating, late-type M dwarfs still show magnetic activity. While differences in the activity fractions between early and late-type M dwarfs have been seen for decades (e.g., Gizis et al. 2000; West et al. 2004) and can be explained by differences in active lifetimes (West et al. 2008), Figure 6 suggests that the relationship between activity and rotation may be different in late-type versus early-type M dwarfs. Specifically, it appears that late-type M dwarfs may stay active at slower rotation speeds than their early-type counterparts.

We also investigated how the strength of magnetic activity (quantified by $L_{\rm H\alpha}/L_{\rm bol}$) varies as a function of rotation period. Figure 7 shows $\log(L_{\rm H\alpha}/L_{\rm bol})$ (filled circles) as a function of

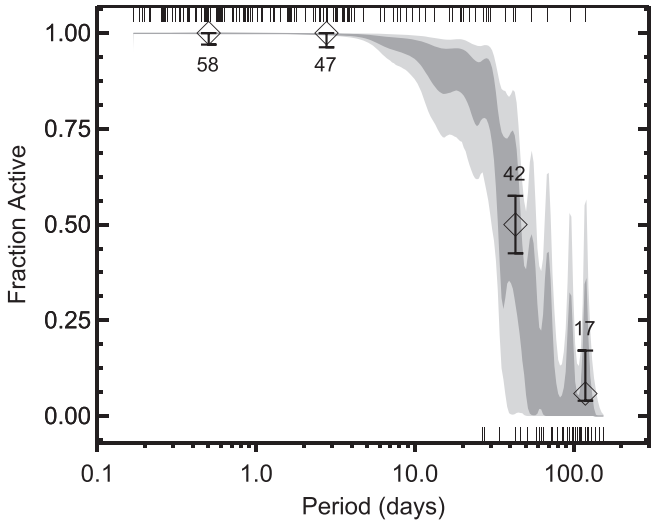

Figure 5. Fraction of magnetically active stars for all M dwarfs in our sample as a function of rotation period. Diamonds represent logarithmically spaced bins with error bars calculated from binomial statistics. The numbers above/below each symbol represent the number of stars in each bin. The gray shaded regions show the nonparametric probability density function of the activity fraction with confidence intervals (dark gray—68%; light gray—95%) determined from 5000 bootstrap samples of the data. Rug plots on the top and bottom indicate the active and inactive (respectively) stars used to compute the activity fraction. All of the fast rotators are active, whereas a small but non-zero fraction of the slow rotators show magnetic activity.

rotation period for early-type (left; M1–M4) and late-type (right; M5–M8) M dwarfs. The inactive stars with measured rotation periods are plotted as open circles. The early-type M dwarfs show a decrease in activity strength with increased rotation period. In contrast, the late-type M dwarfs are consistent with having the same level of activity, except perhaps at the longest rotation periods. To quantify this, we performed a linear least squares fit to the active stars in both panels of Figure 7. In the early-type dwarfs, $\log(L_{\rm H\alpha}/L_{\rm bol})$ shows a statistically significant decrease as function of rotation period, and has the form,

$$\log\left(L_{\rm H\alpha}/L_{\rm bol}\right) = -\ (3.44 \pm 0.023) - (0.19 \pm 0.036) \times \log\left(P_{\rm rot}\right), \quad (3)$$

with $P_{\rm rot}$ as the rotation period in days. For the late-type M dwarfs, $\log(L_{\rm H\alpha}/L_{\rm bol})$ shows no significant trend with rotation period (slope $= -0.016 \pm 0.050$). The slope of the active late-type dwarfs is not consistent with the decreasing trend seen in the active early-type M dwarfs. In both cases, the scatter about the best-fit line is dominated by the intrinsic scatter rather than measurement uncertainty. Binning the data in logarithmic bins of rotation period confirms these bulk trends (Figure 8). Both

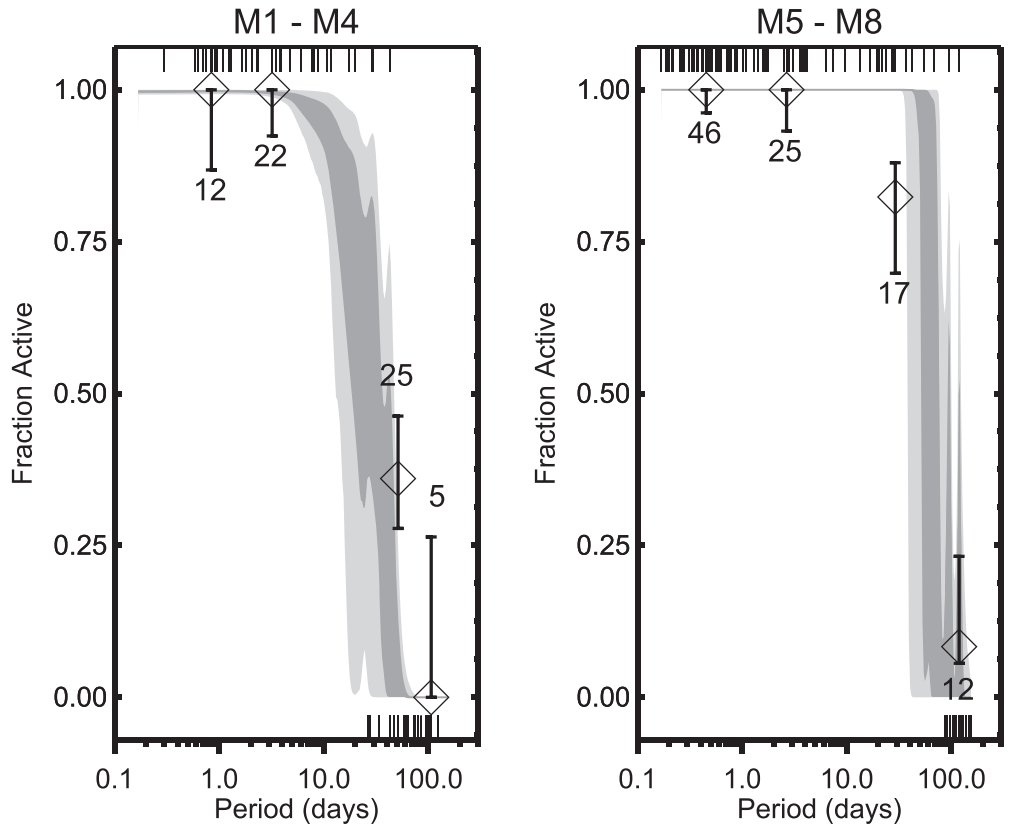

Figure 6. Fraction of active early-type (left) and late-type (right) M dwarfs in our sample as a function of rotation period. Diamonds represent logarithmically spaced bins with error bars calculated from binomial statistics. The numbers above/below each symbol represent the number of stars in each bin. The gray shaded regions show the nonparametric probability density function of the activity fraction with confidence intervals (dark gray—68%; light gray—95%) determined from 2000 bootstrap samples of the data. Rug plots on the top and bottom indicate the active and inactive (respectively) stars used to compute the activity fraction. At similar rotation periods, a much larger fraction of the late-type M dwarfs are active, indicating that the activity–rotation relation in M dwarfs may be mass dependent.

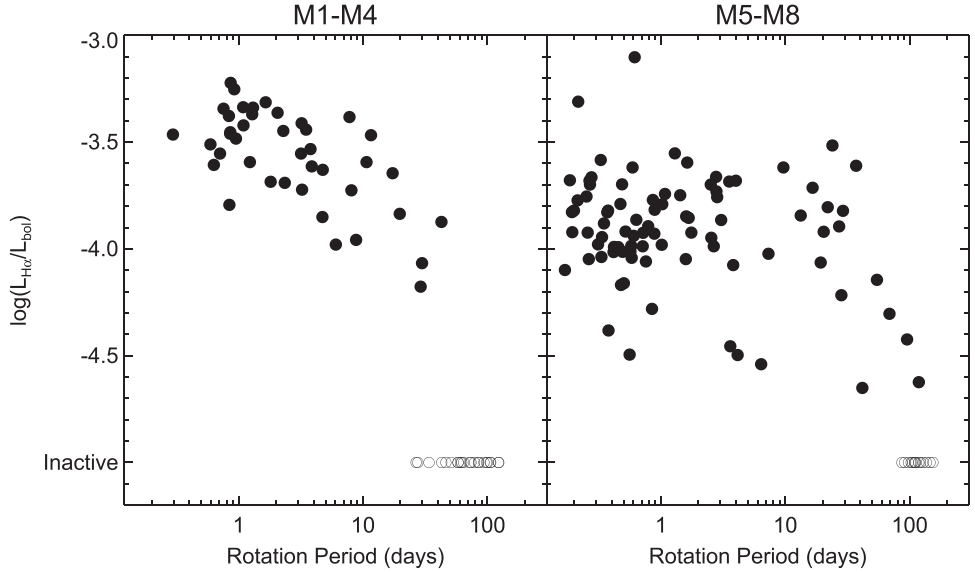

Figure 7. $\log(L_{H\alpha}/L_{bol})$ as a function of rotation period for early-type (left) and late-type (right) M dwarfs (filled circles). Inactive stars with measured rotation periods are included as open circles. In the early-type M dwarfs there is a clear decease in the strength of magnetic activity with increasing rotation period. The late-type M dwarfs are much more scattered, but appear to maintain a similar level of activity except for the very slowest rotators. The inactive stars suggest that there may exist rotation periods (26 days; early-type and 86 days; late-type), faster than which all stars are magnetically active.

Figures 7 and 8 demonstrate that there is a connection between rotation and activity in late-type M dwarfs; all stars rotating with periods shorter than ∼90 days are active. There is also a hint that there may be a correlation between rotation and activity in the late-type M dwarfs with rotation periods longer than 90 days, but there are not enough stars to make any strong conclusions (e.g., the slowest rotation bin of Figure 8 contains only one star). Additional late-type, slowly rotating, active M

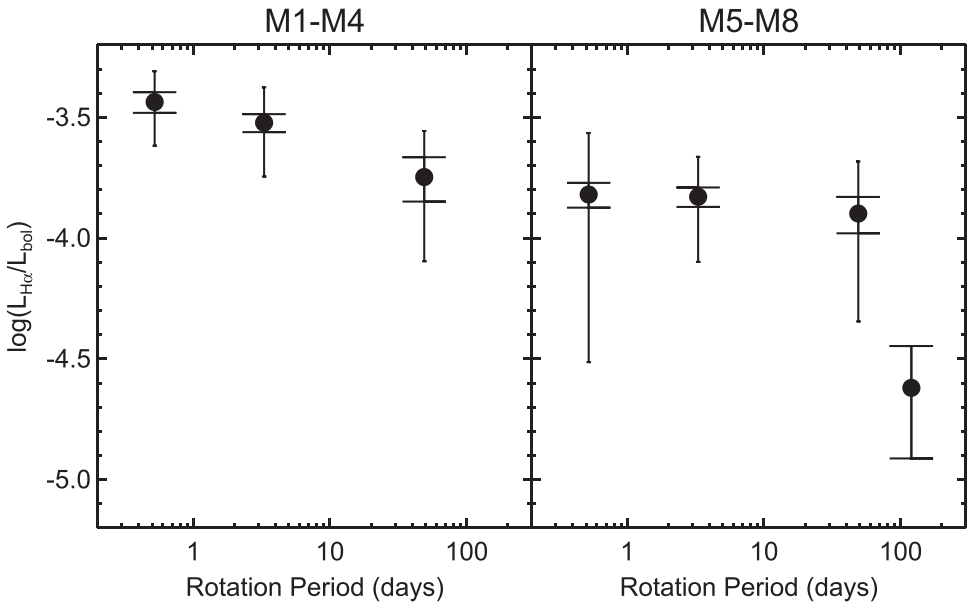

Figure 8. $\log(L_{H\alpha}/L_{bol})$ as a function of rotation period for early-type (left) and late-type (right) M dwarfs. Each data point corresponds to the mean value (of activity and rotation period) for the stars in the bin. The vertical error bars represent the spread of the data (thin bars) and the uncertainty in the mean values (wide bars). Only three bins are shown for the M1–M4 dwarfs, as no active stars of these types were found with periods longer than 100 days. There is only one star in the slowest rotating late-type bin and the error bars on this data point represent the uncertainty in the $L_{H\alpha}/L_{bol}$ measurement. In the early-type M dwarfs there is evidence of a decease in the strength of magnetic activity with increasing rotation periods. This is in contrast to the late-type M dwarfs, which maintain a similar level of activity except for the very slowest rotators.

dwarfs are required to confirm if magnetic activity is weaker in slowly rotating, fully convective M dwarfs.

Figure 7 also suggests that while fast rotation is correlated with magnetic activity in all M dwarfs, there are clear differences between the early and late-type populations. Similar to what was seen in Figure 6, the late-type M dwarfs maintain a high (and comparable) level of magnetic activity until their rotation periods exceed ∼90 days, beyond which the level of activity appears to decrease. In the early-type M dwarfs, there is a much more clear decrease in activity at all rotation periods and an absence of active stars with periods >30 days. The inactive stars in both panels corroborate that rotation plays an important role in the generation of magnetic activity in M dwarfs and hint at the possibility of a rotation threshold faster than which magnetic activity is present. All M dwarfs rotating faster than 26 days and 86 days in the early-type and late-type populations, respectively, are magnetically active.

Figures 7 and 8 also demonstrate an alternative method for studying the range of magnetic activity strengths in M dwarfs. Our results reduce the contribution of different rotation periods to the spread of activity strength and allowed us to examine the intrinsic spread of the population (at a given rotation rate), particularly for early-type M dwarfs. While the mean values have relatively small uncertainties (wide error bars) in most bins, the spread (thin error bars) at each rotation bin remains large (typically about 0.3–0.5 dex). We see that mixing stars of various rotation rates (and perhaps different ages) *does* increase the spread of the population (particularly for early-type M dwarfs). Additionally, some of the spread seen in individual bins in Figure 8 indicate that the M dwarf population has a significant intrinsic variety of activity strengths. As has been seen in previous studies (e.g., Berger et al. 2008; Lee et al. 2010; Bell et al. 2012), much of the observed spread may be due to the Hα variability of individual M dwarfs.

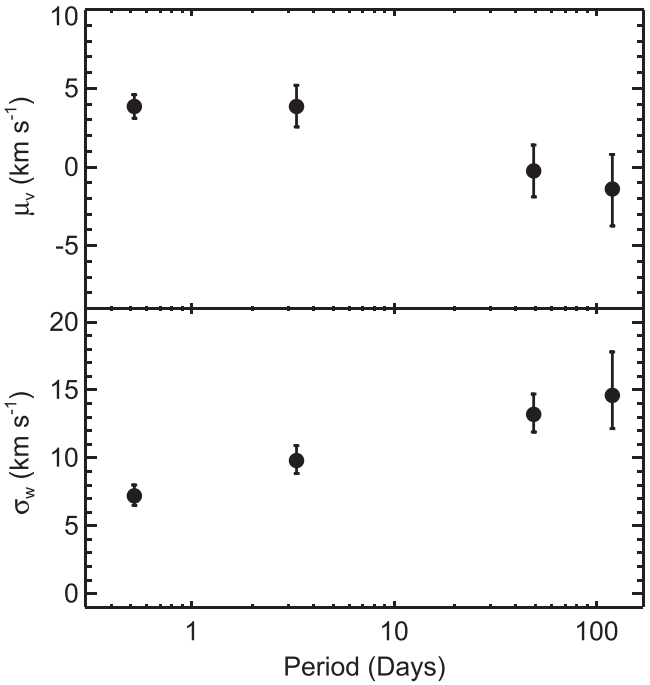

Figure 9. Mean V velocities (top), and W velocity dispersions (bottom) as a function of rotation period. Error bars represent the 1σ uncertainties in each bin. Both panels suggest that slowly rotating M dwarfs are drawn from an older kinematic population.

4.2. Kinematics, Rotation, and Activity

From the results of the kinematic analysis described in Section 3.2, we examined the bulk motions of the sample as a function of rotation period. Figure 9 shows the mean V velocity (top) and the W velocity dispersion (bottom) of the entire sample (relative to the Local Standard of Rest) as a function of rotation period. The V component of the velocity (in the

direction of Galactic rotation) shows clear signs of increasing asymmetric drift with increasing rotation period. Namely, the mean V velocity decreases for stars with slow rotation rates. This decrease is a strong indicator that the population of slow rotators is older; dynamical heating over time causes elliptical orbits, which lead to a bulk decrease in V motion. The mean U and W motions are insensitive to asymmetric drift and provide little information about the ages of small samples of stars. All of the population U, V, and W values (means and dispersions) are included in Table 2 for completeness.

The velocity dispersion of the W component (bottom panel of Figure 9; in the vertical direction, out of the plane of the Galaxy) increases with increasing stellar rotation period. Increases in the vertical velocity dispersion are typically associated with multiple dynamical encounters and older ages. As with the asymmetric drift apparent in the mean velocities, the vertical velocity dispersion measurements suggest that the slower rotators are dynamically older. The dispersions of the U and V components can be affected by other processes and are less directly linked to dynamical heating than the W velocity dispersions, but are also included in Table 2.

We also completed the same kinematic analysis for separated late-type and early-type populations and found no significant differences in their kinematics.

5. CONCLUSIONS AND DISCUSSION

The spectroscopic follow-up of 238 M dwarfs, combined with the rotation rates from the MEarth transit survey has provided an unprecedented sample for examining the rotation, magnetic activity and kinematics of mid-to-late M dwarfs. We conducted an analysis of the magnetic activity properties and investigated the bulk 3D kinematics of the population as a function of rotation. In the spectroscopic sample, 164 stars have measured rotation periods, 160 are magnetically active, and 127 of the M dwarfs are both active and have measured rotation periods. We provide all of the sample and derived quantities in the electronic version of this manuscript.

The results of our analysis are summarized as follows.

1. For early-type M dwarfs, the activity fractions decrease with increasing rotation period. For the late-type M dwarfs, the higher activity fractions extend to slower rotation rates before rapidly declining.
2. All of the rapidly rotating stars are magnetically active, with few (but some) of the slowest rotators showing signs of activity.
3. For early-type (M1–M4) M dwarfs, all stars rotating faster than 26 days are magnetically active, as are all late-type M dwarfs (M5–M8) with rotation periods shorter than 86 days. It is worth noting that for a $0.2\,M_{\odot}$ star, 26 and 86 days correspond to $v \sin i$ values of 0.4 and $0.1\,\mathrm{km\,s^{-1}}$, respectively, both of which are below the detection limits of most spectrographs.
4. At the longest rotation periods, we see no active early-type M dwarfs, but there are a few slowly rotating, active, late-type M dwarfs.
5. The strength of magnetic activity appears to decline with increased rotation period in early-type M dwarfs. The fully convective, late-type M dwarfs remain at a similar activity level as rotation slows, perhaps until the slowest rotation periods (>90 days).
6. From our kinematic analysis, it appears that M dwarfs with longer rotation periods are drawn from a kinematically older population. Specifically, we see that slowly rotating stars exhibit signs of asymmetric drift and have larger velocity dispersions about the mid-plane, both signs of dynamically heated, older populations.
7. There are a few slowly rotating M dwarfs that show signs of magnetic activity, and which may provide important laboratories for additional investigations about the role rotation plays in the magnetic field generation in low-mass stars.

In general, we find a strong relationship between rotation and activity for early-type M dwarfs. The relationship is much less pronounced, but appears to exist for the late-type M dwarfs that are fully convective. For all M dwarfs, rotation appears to affect the presence of activity; fast rotators are more likely to show strong activity, while slow rotators are less likely to be active. However, in the late-type M dwarfs, magnetic activity appears to be present in stars with slower rotation than their early-type counterparts. Larger samples that include measurements of magnetic activity and rotation are required to further investigate this discrepancy (e.g., Newton et al. 2015, in preparation).

Our kinematic analysis suggests that rotation is linked to age in all M dwarfs. We conclude that younger M dwarfs (both early and late-type) are rotating faster and more likely to be active. Future analysis of wide binaries (particularly those with a white dwarf companion from which we can determine age) and/or stellar clusters will provide better information about the detailed role that stellar age plays in the observed rotation and magnetic activity of low-mass stars.

While our kinematic analysis shows clear signs of asymmetric drift and dynamical heating, the magnitudes of the effects are far less than what is seen in large samples of M dwarfs that probe farther into the Milky Way disk (e.g., Bochanski et al. 2007a). This suggests that the slow rotators in our sample are older than the fast rotators, but that they are still younger than typical old stellar populations in the Galactic (thin) disk. This is not surprising given that the MEarth targets are selected to be nearby, where it is much more likely to sample a younger population (West et al. 2008).

Some of the active stars in our spectroscopic sample do not have measured rotation periods (21%) and were therefore not included in some of our analyses. 74 stars in the sample do not have rotation periods (55% of which are inactive). Because our ability to measure a rotation rate of an M dwarf depends on the presence of starspots, it is not surprising that some stars, namely the inactive ones, may not show rotational modulation; indeed, the majority of the stars with rotation periods are active (77%). However, the lack of measured rotation in the active stars could be due to a number of effects, including but not limited to, homogeneous spot geometry, short-lived spots, insensitivity to low-amplitude variations (few small spots), or an over abundance of spots. The latter effect would cause a decrease in the rotational modulation for the most active (heavily spotted) stars. We ran the non-rotating stars through our kinematic analysis (53 have 3D kinematics) and found that as a population they are consistent with M dwarfs in the 10–100 day rotation bins. We conclude that kinematically, the stars without rotation measurements could be on the older end of the spectrum for our sample. The active fractions of early and late-type M dwarfs without rotation measurements are

consistent with the entire sample in the 10–100 day rotation bins. Therefore, the exclusion of the active stars without rotation measurements does not likely effect our results, but may be explored in a future study when we can ascertain the reason for the lack of rotational modulation.

The fact that there are a small number of active, slowly rotating, late-type M dwarfs in our sample suggests that the activity–rotation relation may be more complicated than predicted by a simple spin-down model. One possibility could be that while persistent magnetic activity in late-type M dwarfs is rare (or non-existent) for slow rotators, the presence of magnetic cycles may produce observed activity in a small number of stars at any given time. Long-term observations are required to further test this hypothesis. The small number of active, slowly rotating, late-type M dwarfs could also be due to the young bias of MEarth, which might exclude such stars. An additional factor that could influence our analysis is the potential presence of close binary companions, which have been shown to affect the magnetic activity (and rotation) of stars (e.g., Morgan et al. 2012). While multiplicity likely plays a minor role due to the small binary fraction of M dwarfs (Fischer & Marcy 1992), high resolution imaging and/or spectroscopy would be required to further investigate its role.

Our analysis divided M dwarfs into early (M1–M4) and late-types (M5–M8) and did not explore the ramifcations of altering the boundary between the two populations. Ideally, we would conduct the analysis as a function of spectral type but we did not have enough stars in each spectral type to produce a statistically significant result. As stated above, our analysis is therefore mostly a comparison between M3–M4 and M5–M6 dwarfs. Future and ongoing studies will provide additional time-series photometric data with which we can further study the rotation and activity behavior of M dwarfs (over a larger range of spectral types), both surveys such as MEarth (both north and south; Irwin et al. 2014), APACHE (Sozzetti et al. 2013), SPECULOOS (Gillon et al. 2013), and ExTrA[10] that focus specifically on M dwarfs and more general photometric surveys like Pan-STARRS (Kaiser et al. 2002) and LSST (Ivezic et al. 2008).

The authors acknowledge Elisabeth Newton, Dylan Morgan, and the other members of the Boston Area Drinking And Society for Stars of Elfin Stature for useful conversations in the preparation of this manuscript. A.A.W. acknowledges the support of NSF grants AST-1109273 and AST-1255568 and the Research Corporation for Science Advancement's Cottrell Scholarship. K.L.W. acknowledges the support of the Boston University UROP program and the Clare Boothe Luce scholarship. Z.K.B.T. gratefully acknowledges support from the Torres Fellowship for Exoplanetary Research. The MEarth Team gratefully acknowledges funding from the David and Lucille Packard Fellowship for Science and Engineering (awarded to D.C.). This material is based upon work supported by the National Science Foundation under grants AST-0807690, AST-1109468, and AST-1004488 (Alan T. Waterman Award). This publication was made possible through the support of a grant from the John Templeton Foundation. The opinions expressed in this publication are those of the authors and do not necessarily reflect the views of the John Templeton Foundation. This material is based upon work supported by the National Science Foundation Graduate Research Fellowship (to JSP) under grant No. DGE-1144469.

[10] http://www.eso.org/sci/meetings/2014/exoelt2014/presentations/Bonfils.pdf

REFERENCES

Barnes, S. A. 2003, ApJ, 586, 464
Barry, D. C. 1988, ApJ, 334, 436
Bell, K. J., Hilton, E. J., Davenport, J. R. A., et al. 2012, PASP, 124, 14
Berger, E., Gizis, J. E., Giampapa, M. S., et al. 2008, ApJ, 673, 1080
Berta, Z. K., Irwin, J., Charbonneau, D., Burke, C. J., & Falco, E. E. 2012, AJ, 144, 145
Bochanski, J. J., Munn, J. A., Hawley, S. L., et al. 2007a, AJ, 134, 2418
Bochanski, J. J., West, A. A., Hawley, S. L., & Covey, K. R. 2007b, AJ, 133, 531
Browning, M. K. 2008, ApJ, 676, 1262
Browning, M. K., Basri, G., Marcy, G. W., West, A. A., & Zhang, J. 2010, AJ, 139, 504
Burgasser, A. J., Liebert, J., Kirkpatrick, J. D., & Gizis, J. E. 2002, AJ, 123, 2744
Chabrier, G., & Baraffe, I. 1997, A&A, 327, 1039
Charbonneau, D., Berta, Z. K., Irwin, J., et al. 2009, Natur, 462, 891
Covey, K. R., Ivezic, Z., Schlegel, D., et al. 2007, AJ, 134, 2398
Delfosse, X., Forveille, T., Perrier, C., & Mayor, M. 1998, A&A, 331, 581
Dittmann, J. A., Irwin, J. M., Charbonneau, D., & Berta-Thompson, Z. K. 2014, ApJ, 784, 156
Dobler, W., Stix, M., & Brandenburg, A. 2006, ApJ, 638, 336
Dressing, C. D., & Charbonneau, D. 2013, ApJ, 767, 95
Dressing, C. D., & Charbonneau, D. 2015, ApJ, 807, 45
Eggen, O. J., & Iben, I., Jr. 1989, AJ, 97, 431
Fischer, D. A., & Marcy, G. W. 1992, ApJ, 396, 178
Gillon, M., Jehin, E., Delrez, L., et al. 2013, Protostars and Planets VI Posters, 2K066
Gizis, J. E., Monet, D. G., Reid, I. N., et al. 2000, AJ, 120, 1085
Hawley, S. L., Gizis, J. E., & Reid, I. N. 1996, AJ, 112, 2799
Hawley, S. L., Tourtellot, J. G., & Reid, I. N. 1999, AJ, 117, 1341
Irwin, J., Aigrain, S., Bouvier, J., et al. 2009a, MNRAS, 392, 1456
Irwin, J., Berta, Z. K., Burke, C. J., et al. 2011a, ApJ, 727, 56
Irwin, J. M., Berta, Z. K., Burke, C. J., et al. 2011b, ApJ, 742, 123
Irwin, J. M., Berta-Thompson, Z. K., Charbonneau, D., et al. 2014, arXiv:1409.0891
Irwin, J., Charbonneau, D., Berta, Z. K., et al. 2009b, ApJ, 701, 1436
Ivezic, Z., Tyson, J. A., Abel, B., et al. 2008, arXiv:0805.2366
Kaiser, N., Aussel, H., Burke, B. E., et al. 2002, Proc. SPIE, 4836, 154
Kiraga, M., & Stepien, K. 2007, AcA, 57, 149
Koenker, R. 2015, Quantreg Quantile Regression r Package Version 5.11
Law, N. M., Kraus, A. L., Street, R., et al. 2012, ApJ, 757, 133
Lee, K.-G., Berger, E., & Knapp, G. R. 2010, ApJ, 708, 1482
Leggett, S. K. 1992, ApJS, 82, 351
Lépine, S., Rich, R. M., & Shara, M. M. 2005, ApJL, 633, L121
Lépine, S., & Shara, M. M. 2005, AJ, 129, 1483
Mamajek, E. E., & Hillenbrand, L. A. 2008, ApJ, 687, 1264
Mohanty, S., & Basri, G. 2003, ApJ, 583, 451
Montes, D., López-Santiago, J., Gálvez, M. C., et al. 2001, MNRAS, 328, 45
Morgan, D. P., West, A. A., Garcés, A., et al. 2012, AJ, 144, 93
Muirhead, P. S., Hamren, K., Schlawin, E., et al. 2012, ApJL, 750, L37
Newton, E. R., Charbonneau, D., Irwin, J., et al. 2014, AJ, 147, 20
Nidever, D. L., Marcy, G. W., Butler, R. P., Fischer, D. A., & Vogt, S. S. 2002, ApJS, 141, 503
Nutzman, P., & Charbonneau, D. 2008, PASP, 120, 317
Pizzolato, N., Maggio, A., Micela, G., Sciortino, S., & Ventura, P. 2003, A&A, 397, 147
R Core Team 2014, R: A Language and Environment for Statistical Computing (Vienna, Austria: R Foundation for Statistical Computing)
Reid, I. N., & Hawley, S. L. 2005, New Light on Dark Stars: Red Dwarfs, Low-mass Stars, Brown Dwarfs (Chichester: Praxis Publishing Ltd.)
Reid, I. N., Hawley, S. L., & Gizis, J. E. 1995, AJ, 110, 1838
Reiners, A., & Basri, G. 2008, ApJ, 684, 1390
Reiners, A., & Basri, G. 2009, ApJ, 705, 1416
Reiners, A., & Mohanty, S. 2012, ApJ, 746, 43
Schönrich, R., Binney, J., & Dehnen, W. 2010, MNRAS, 403, 1829
Shkolnik, E. L., Hebb, L., Liu, M. C., Reid, I. N., & Collier Cameron, A. 2010, ApJ, 716, 1522
Silvestri, N. M., Hawley, S. L., & Oswalt, T. D. 2005, AJ, 129, 2428
Skumanich, A. 1972, ApJ, 171, 565
Soderblom, D. R. 2010, ARA&A, 48, 581
Soderblom, D. R., Duncan, D. K., & Johnson, D. R. H. 1991, ApJ, 375, 722

Sozzetti, A., Bernagozzi, A., Bertolini, E., et al. 2013, in European Physical Journal Web of Conf., 47, 3006
Stauffer, J. R., Caillault, J.-P., Gagne, M., Prosser, C. F., & Hartmann, L. W. 1994, ApJS, 91, 625
Stauffer, J. R., & Hartmann, L. W. 1986, ApJS, 61, 531
Walkowicz, L. M., & Hawley, S. L. 2009, AJ, 137, 3297
Walkowicz, L. M., Hawley, S. L., & West, A. A. 2004, PASP, 116, 1105
West, A. A., & Basri, G. 2009, ApJ, 693, 1283
West, A. A., Bochanski, J. J., Hawley, S. L., et al. 2006, AJ, 132, 2507
West, A. A., Hawley, S. L., Bochanski, J. J., et al. 2008, AJ, 135, 785
West, A. A., Hawley, S. L., Walkowicz, L. M., et al. 2004, AJ, 128, 426
West, A. A., Morgan, D. P., Bochanski, J. J., et al. 2011, AJ, 141, 97
Williams, P. K. G., Berger, E., Irwin, J., Berta-Thompson, Z. K., & Charbonneau, D. 2014, ApJ, 799, 192
Wilson, O., & Woolley, R. 1970, MNRAS, 148, 463
York, D. G., Adelman, J., Anderson, J. E., Jr., et al. 2000, AJ, 120, 1579